Supporting Information

Erythrocyte Membrane Is an Alternative Coating to Polyethylene Glycol for Prolonging the Circulation Lifetime of Gold Nanocages for Photothermal Therapy

Ji-Gang Piao, [§¶‡] *Limin Wang,* [¶‡] *Feng Gao,* [¶†] *Ye-Zi You,** [§¶] *Yujie Xiong,** [¶] *Lihua Yang** [§¶]

[§] CAS Key Laboratory of Soft Matter Chemistry, [¶] School of Chemistry and Materials Science, [†] CAS Key Laboratory of Materials for Energy Conversion, University of Science and Technology of China, Hefei, Anhui 230026 China

‡ These authors contributed equally to this work.

* Corresponding authors: (L. Y.) lhyang@ustc.edu.cn; (Y. X.) yjxiong@ustc.edu.cn; (Y.-Z. Y.) yzyou@ustc.edu.cn

Additional Figures

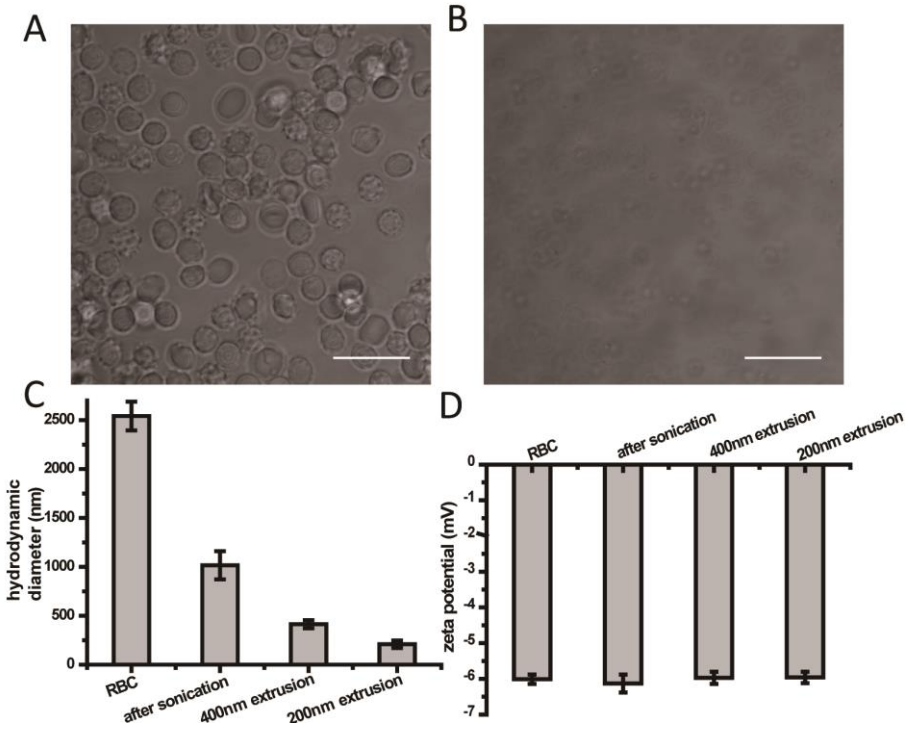

Figure S1. (A-B) Differential Interference Contrast (DIC) images of mouse RBCs before (A) and after (B) hypotonic treatment. Change in DIC indicates an alteration of the medium inside the RBCs, suggesting successful deprivation of RBC interior contents. Scale bar = 25 μm. (C-D) The average hydrodynamic diameters (C) and zeta potentials (D) of the RBC-membrane-derived vesicles following RBC ghosts derivation, sonication for 5 min, extrusion through 400-nm polycarbonate porous membranes, and extrusion through 200-nm polycarbonate porous membranes. Data points are reported as mean ± standard deviation.

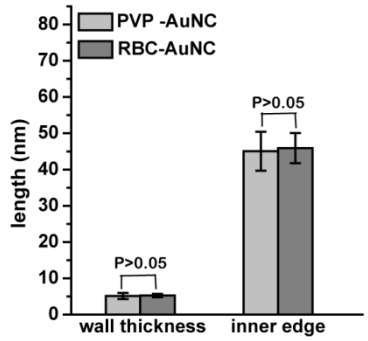

Figure S2. The average Au-wall thickness and the average inner edge length of AuNCs before (*i.e.*, PVP-AuNC) and after (*i.e.*, RBC-AuNC) the vesicle-AuNC fusion step, averaged over 40 and 30 nanoparticles, respectively, based on their corresponding TEM images. Clearly, both the average inner edge length and average Au-wall thickness of the RBC-AuNCs are close to those of the PVP-AuNCs without biostatistical difference ($p > 0.05$). Data points are reported as mean ± standard deviation.

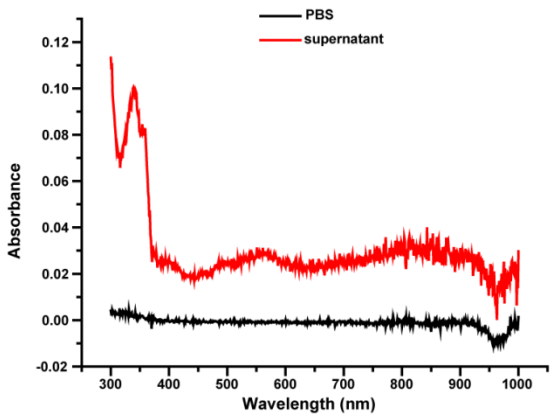

Figure S3. UV-vis-NIR absorption spectrum of the supernatant post the vesicle-AuNC fusion. The absence of the LSPR peak characteristic of AuNCs indicates recovery of most RBC-AuNCs in the pellet, and the presence of strong absorption in the UV region, which corresponds well to that characteristic of RBC

membranes, indicate successful removal of excess RBC-membrane-derived vesicles. UV-vis-NIR absorption spectrum of PBS is included as a control.

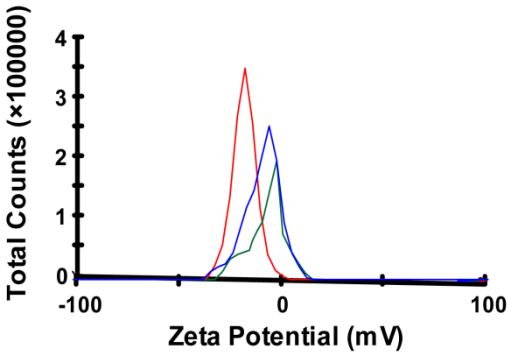

Figure S4. The distributions of zeta potential by number of particles for AuNCs before (red) and after (blue) the vesicle-AuNC fusion step. That for RBC-membrane-derived vesicles (green) is included as a reference.

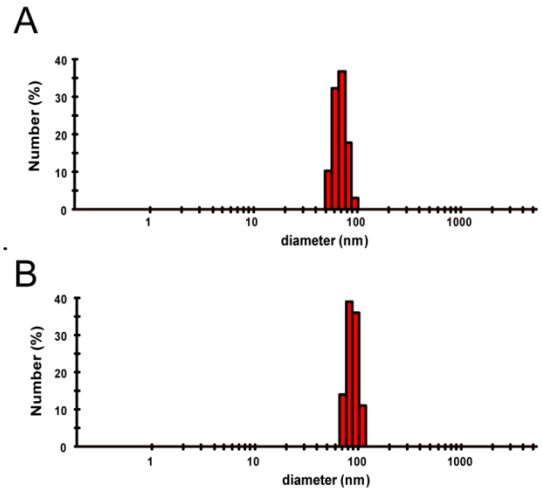

Figure S5. (A-B) The distributions of hydrodynamic diameter by number of particles for AuNCs before (A) and after (B) the vesicle-AuNC fusion step, measured with dynamic light scattering (DLS).

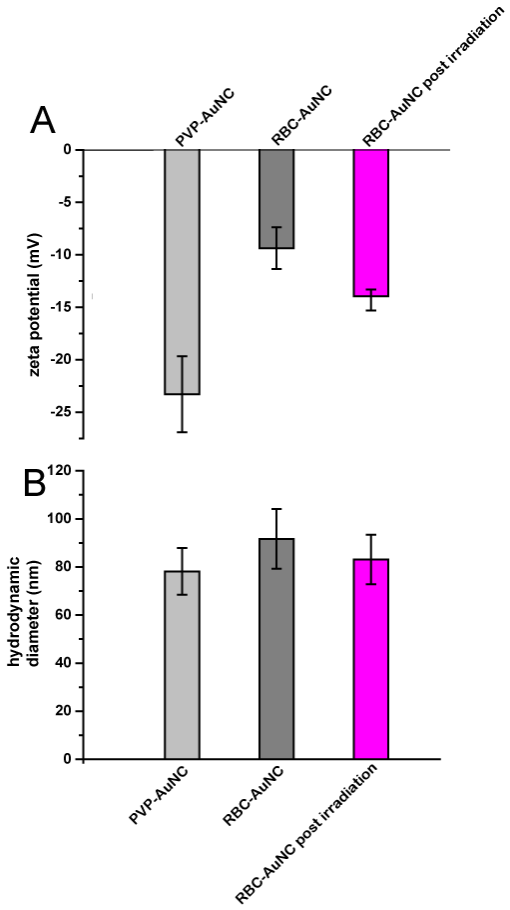

Figure S6. The average zeta potential (A) and average hydrodynamic diameter (B) of RBC-AuNCs before and after NIR irradiation with an 850-nm laser at 1 W/cm^2 for 5 min, with those of the PVP-AuNCs included as a reference. The NIR irradiation renders both the average zeta potential (A) and the average hydrodynamic diameter (B) of RBC-AuNCs slightly shift from those of non-irradiated RBC-AuNCs toward those of the pristine PVP-AuNCs, indicative of partial ablation of the RBC-membranes by the NIR irradiation. Data points are reported as mean ± standard deviation.

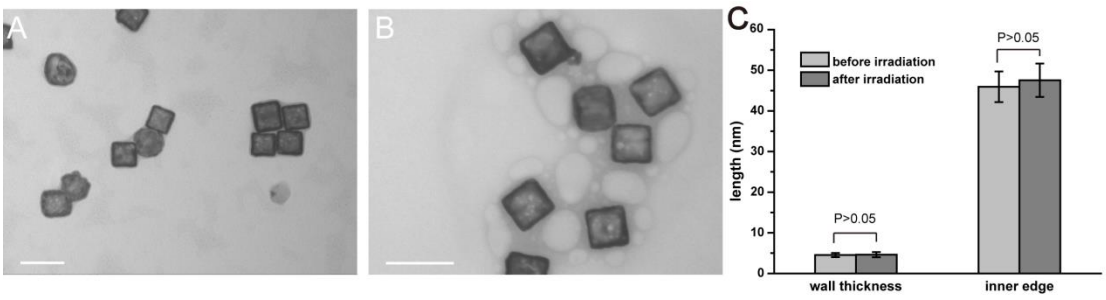

Figure S7. (A-B) TEM images of RBC-AuNCs before (A) and after (B) NIR irradiation with an 850-nm laser at 1 W/cm^2 for 10 min. Scale bar = 100 nm. (C) The average Au-wall thickness and the average inner edge length of the hollow AuNC-core of RBC-AuNCs before and after NIR irradiation, averaged over 14 and 12 nanoparticles, respectively, based on their corresponding TEM images. Clearly, the average outer edge length of the irradiated RBC-AuNCs is close to that of the non-irradiated RBC-AuNCs without biostatistical difference ($p > 0.05$). Data points are reported as mean ± standard deviation.

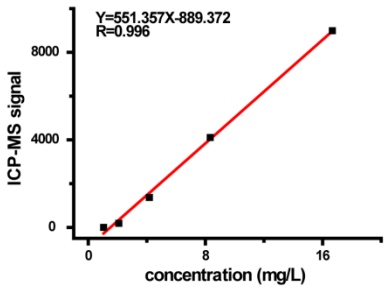

Figure S8. The calibration curve of ICP-MS signal *versus* Au concentration, measured on solutions with known Au concentrations.

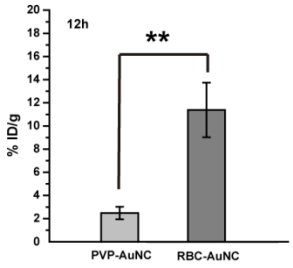

Figure S9. Blood retentions of the RBC-AuNCs and the pristine PVP- AuNCs at 12-h post injection. AuNCs were injected into mice through tail-vein and, at 12-h post AuNC injection, blood was withdrawn from mouse tail-vein and Au contents in blood were determined with ICP-MS. Data points are reported as mean ± standard deviation. ** indicates $p < 0.01$.

Additional Results and Discussion

Estimation on the difference in tumor uptake expressed in particle numbers. In the biodistribution studies, the dosages of AuNC dispersions we injected into each mouse are kept constant at Au dose of ~0.25 mg, which corresponds to approximately 10^{12} AuNC particles per injection. At 48-h post injection, the tumor uptakes in mice injected with the RBC-AuNCs and the PVP-AuNCs are 7.77 ± 2.31 and 4.46 ± 1.46 % ID/g, respectively. At this time-point, the average tumor masses of mice injected with the RBC-AuNCs and the PVP-AuNCs are 1.34 ± 0.11 and 1.12 ± 0.15 g, respectively. Therefore, the numbers of RBC-AuNC and PVP-AuNC particles accumulated within tumor are estimated to be ~10×10^{10} and ~5.0×10^{10}, respectively. Thus, a seemingly small difference in tumor uptake when expressed in %

ID/g—approximately 3.3% ID/g—actually corresponds to a huge difference when expressed in number of particles accumulated within tumor—on the scale of 10^{10} particles. Note that the AuNC aqueous dispersions used for the *in vitro* photothermal conversion experiments contain approximately 10^{10} AuNC-particles/mL and, after irradiation at 1 W/cm^2 for 5 min, demonstrate temperature rises of ~15 °C. Therefore, a difference of ~3.3% ID/g in tumor uptake for the RBC-AuNCs *versus* the PVP-AuNCs may lead to appreciable difference in temperature rise at tumor site when applied for *in vivo* PTT cancer treatment.